Analytic nearest-neighbor model for fcc metals

R. A. Johnson

Department of Materials Science, University of Virginia, Thornton Hall, Charlottesville, Virginia 22901

The implications of the mathematical format of the embedded-atom method of computer modeling of metals have been studied with use of a simple nearest-neighbor analytic model for the fcc lattice. The physical inputs into the model are the atomic volume, the cohesive energy, the bulk modulus, the average shear modulus, the vacancy-formation energy, and the slope at the nearest-neighbor distance of the spherically averaged free-atom electron density calculated with Hartree-Fock theory. The model employs an exponential repulsion between nearest-neighboring atoms, an exponentially decreasing function for the free-atom electron density, and a universal equation relating the crystal energy and the lattice constant. The anisotropy ratio of the cubic shear moduli is constrained to be 2 with this model. The dependence of the energies for unrelaxed configurations for vacancy formation, divacancy binding, and low-index plane surfaces on the model parameters has been analyzed. The average shear modulus plays a dominant role in determining these energies relative to the bulk modulus or the cohesive energy because the slope of the embedding function at the equilibrium electron density is linear in the average shear modulus. Embedding functions are not uniquely determined in specific models, and it is shown that the embedding functions used in several models are essentially equivalent.

I. INTRODUCTION

Metals have been studied with calculations based on computer models since the earliest availability of digital computers for scientific research. Fundamental to any such research is the choice of the manner in which atoms interact, i.e., of an interatomic potential. Numerous approaches have been used, leading to a long bibliography[1-5] and a full complement of controversy. Any choice is an approximation, so there is no ideal way of treating this problem. Simple potentials tend not to have enough flexibility to accurately portray real metals, while more fundamental approaches tend to be too unwieldy to carry out the desired calculations with sufficient efficiency.

A new procedure for designing a mathematical model of a metal has been developed by workers at Sandia National Laboratory called the embedded-atom method (EAM).[6,7] It is based on density-functional theory as derived by Stott and Zaremba (quasiatom approach)[8] and Nørskov and Lang (effective-medium approach).[9] Here the energy required to place a small impurity atom in a lattice is taken solely as a function of the electron density at that particular site. Each atomic species therefore has a unique energy function which is in turn a function of just the electron density. For example, Puska et al.[10] have calculated this function for a number of light atoms using a constant electron density (jellium) formulation. Daw and Baskes[6,7] extended this idea to a general lattice model which permits variation in atomic positions by also including a two-body central interatomic potential. Thus it has been possible to include lattice relaxation and cover a broad range of metals, impurities, and alloys, including bulk, surface, and liquid properties.[6,7,11-18] Results have been encouraging in that the model has shown satisfactory agreement with experimental data over a spectrum of (often previously intractable) problems.

As presently used, there is appreciable numerical fitting to obtain the parameters and functions required for an EAM model and all results must be obtained by numerical calculations. To study the relationships between the physical input and output and the model parameters, a simple analytic fcc model has been developed. The derivation of the model is given in the first section below. The model is then applied to several defects to obtain the functional dependence of the energy on the physical parameters through rapidly convergent series expansions.

II. THEORY

A. Embedded-atom method

The basic equations of the embedded-atom method are[7]

$$E_{\text{tot}} = \sum_i F_i(\rho_{h,i}) + \frac{1}{2} \sum_{\substack{i,j \\ (i \neq j)}} \phi_{ij}(R_{ij}) , \tag{1}$$

$$\rho_{h,i} = \sum_{j \, (\neq i)} f_j(R_{ij}) , \tag{2}$$

where E_{tot} is the total internal energy, $\rho_{h,i}$ is the electron density at atom i due to all other atoms, f_j is the electron density of atom j as a function of distance from its center, R_{ij} is the separation distance between atoms i and j, $F_i(\rho_{h,i})$ is the energy to embed atom i in an electron density $\rho_{h,i}$, and ϕ_{ij} is a two-body central potential between atoms i and j. Thus the host electron density $\rho_{h,i}$ is assumed to be a linear superposition of contributions from individual atoms, which in turn are assumed to be spheri-

cally symmetric, and the embedding energy is assumed to be independent of the electron distribution or gradients.

These equations are identical in form to those recently proposed by Finnis and Sinclair,[19] also for an atomistic model for metals. The interpretation is quite different, however: The Finnis and Sinclair derivation is based on tight-binding theory, with $F_i(\alpha_i)$ proportional to the square root of α_i and α_i being the linear superposition of squares of overlap integrals.

To use the embedded-atom method in a lattice model calculation, the f and F functions must be specified for each atomic species, and ϕ for each possible combination of atomic species. Although much of the power of EAM is associated with its utility in the treatment of alloys, a monatomic metal has been assumed in the present work to minimize the number of functions involved with a given calculation. Then, the basic equations, applied to a perfect crystal, can be simplified to

$$E_{\text{tot}} = NE \ , \tag{3}$$

$$E = F(\rho) + \tfrac{1}{2} \sum_m \phi(r_m) \ , \tag{4}$$

$$\rho = \sum_m f(r_m) \ , \tag{5}$$

with N the number of atoms in the crystal, E the energy per atom, i.e., the negative of the cohesive energy, and r_m the mth neighbor to some particular atom.

If the perfect crystal structure is maintained, i.e., the atomic volume is permitted to vary but there are no defects and no shears, then Eq. (4) can be written as

$$E(r_1) = F(\rho(r_1)) + \Phi(r_1) \tag{6}$$

with

$$\Phi(r_1) = \tfrac{1}{2} \sum_m \phi(r_m) \ . \tag{7}$$

Since all neighbor distances are an exact factor times the nearest-neighbor distance, both ρ and Φ are functions of just the atomic volume, or, given the lattice structure, of the nearest-neighbor distance. Using subscript e to indicate evaluation at equilibrium, the experimental cohesive energy E_c is determined by

$$E_e = -E_c = F(\rho_e) + \Phi_e \tag{8}$$

and the equilibrium condition is

$$\left. \frac{d\Phi}{dr_1} \right|_e + \left. \frac{d\rho}{dr_1} \right|_e \left. \frac{dF}{d\rho} \right|_e = 0$$

or

$$\Phi'_e + \rho'_e F'_e = 0 \ . \tag{9}$$

In early EAM calculations, the embedding function was determined by a complex fitting procedure. Foiles[15] has recently introduced a straightforward scheme which is also used in the present model. Rose et al.[20] have shown that, for a broad range of materials, the energy as a function of nearest-neighbor distance (or any length parameter in the lattice) is well approximated by the relation

$$E(r_1) = -E_c \left[1 + \alpha \left[\frac{r_1}{r_{1e}} - 1 \right] \right] \exp \left[-\alpha \left[\frac{r_1}{r_{1e}} - 1 \right] \right] \tag{10}$$

with

$$\alpha = 3 \left[\frac{\Omega_e B_e}{E_c} \right]^{1/2} , \tag{11}$$

where Ω is the atomic volume and B the bulk modulus. Equations (6) and (10) can then be combined to give

$$F(r_1) = -E_c \left[1 + \alpha \left[\frac{r_1}{r_{1e}} - 1 \right] \right]$$
$$\times \exp \left[-\alpha \left[\frac{r_1}{r_{1e}} - 1 \right] \right] - \Phi(r_1) \ . \tag{12}$$

To obtain the embedding function F as a function of ρ, $\rho(r_1)$ must be inverted to give r_1 as a function of ρ. This is then substituted into Eq. (12) for the required relation.

To summarize, the direct physical parameters required for this EAM model are the equilibrium atomic volume, the cohesive energy, and the bulk modulus, as well as the lattice structure. A two-body potential and an electron density function must also be specified to completely define the model. The cohesive energy, bulk modulus, and equilibrium condition [Eq. (9)] are all automatically satisfied through the use of the function of Rose et al.

B. Short-ranged fcc model

To obtain a useful analytic model, simple analytic forms must be chosen for the two-body potential $\phi(r_m)$ and the electron density function $f(r_m)$. Furthermore, it must be possible to invert Eq. (5) for the perfect crystal to obtain an analytic expression for $r_m(\rho)$.

In order to provide a direct procedure for satisfying this last criterion, it is assumed that only nearest neighbors contribute to the electron density and the two-body potential in the fcc lattice. While EAM does not intrinsically require short-ranged interactions, the nearest-neighbor contribution is certainly dominant in the EAM calculations to date. Thus this approximation limits the generality of the model, but should retain the first-order effects. For the perfect crystal, Eqs. (5) and (7) are then

$$\rho(r_1) = 12 f(r_1) \ , \tag{13}$$

$$\Phi(r_1) = 6\phi(r_1) \ . \tag{14}$$

To obtain equations for the elastic constants, the perfect-crystal requirement can be relaxed to permit homogeneous deformations. For the present case, the equations given by Daw and Baskes[7] reduce to

$$C_{11} = X_a + X_b \quad \text{or} \quad B = \tfrac{2}{3} X_a + X_b \ ,$$

$$C_{12} = \tfrac{1}{2} X_a + X_b \quad \text{or} \quad C = \tfrac{1}{2} X_a \ , \tag{15}$$

$$C_{44} = \tfrac{1}{2} X_a \quad \text{or} \quad C' = \tfrac{1}{4} X_a$$

with

$$X_a = \frac{a_e^2}{2\Omega_e} \left[\left[\phi_{1e}'' - \frac{1}{r_{1e}}\phi_{1e}' \right] + 2F_e' \left[f_{1e}'' - \frac{1}{r_{1e}}f_{1e}' \right] \right] , \quad (16)$$

$$X_b = \frac{8a_e^2}{\Omega_e}(f_{1e}')^2 F_e'' . \quad (17)$$

As mentioned above, the bulk modulus $B = (C_{11} + 2C_{12})/3$ is matched exactly. The anisotropy ratio $A = C/C'$ of the two cubic shears $C = C_{44}$ and $C' = (C_{11} - C_{12})/2$ is constrained to be 2 with this model. Thus the elastic constants cannot be fitted exactly with a nearest-neighbor fcc EAM model, independent of the analytic form of $\phi(r)$ and $f(r)$. The experimental anisotropy ratios for six fcc metals used in EAM calculations by Foiles et al.[16] range from 1.59 to 3.19. While this discrepancy appears to be severe, it should be pointed out that the anisotropy ratio is a very delicate parameter, is not usually checked, and is commonly in error in most models. In the present case, the Voigt average shear constant $G = (3C + 2C')/5$ can be matched exactly, while the variation with orientation, although not precise, has the correct sense. The volume dependence of the model occurs through the X_b term.

In prior EAM calculations, the atomic electron densities have been assumed to be well represented by the spherically averaged free-atom densities calculated from Hartree-Fock theory by Clementi and Roetti[21] and McClean and McClean,[22] with an additional adjustable parameter to account for an admixture of different electronic configurations. When these Hartree-Fock electronic densities are plotted, it is seen that they are quite well approximated by a single exponential term in the range of distances of interest in EAM calculations. Thus the electronic density in the present model is taken as

$$f(r) = f_e \exp\left[-\beta\left[\frac{r_1}{r_{1e}} - 1 \right] \right], \quad r \leq r_c \quad (18)$$

where r_c is a cutoff parameter. The two-body potential is taken as a Born-Mayer repulsion, i.e., to have the same analytic form as $f(r)$:

$$\phi(r) = \phi_e \exp\left[-\gamma\left[\frac{r_1}{r_{1e}} - 1 \right] \right], \quad r \leq r_c . \quad (19)$$

With these two equations, the model is complete and the embedding function is

$$F(\rho) = -E_c \left[1 - \frac{\alpha}{\beta}\ln\left[\frac{\rho}{\rho_e} \right] \right] \left[\frac{\rho}{\rho_e} \right]^{\alpha/\beta}$$

$$-\Phi_e\left[\frac{\rho}{\rho_e} \right]^{\gamma/\beta}, \quad (20)$$

where $\rho_e = 12f_e$ and $\Phi_e = 6\phi_e$. Because only ratios of electronic densities occur in Eq. (20), the parameter f_e cancels from the model. There are still four parameters introduced here: ϕ_e, β, γ, and r_c. Although β can be obtained from fitting atomic electron densities, it can also be treated as an adjustable parameter. For the elastic constants or for any defect calculation in which the relax-

ations are small, the exact choice of r_c plays no role as long as the cutoff is well within the gap between first and second neighbors. The calculations discussed later are in this category. Also, the embedding function is not defined for very small electron densities, i.e., for $\rho < \rho_e \exp[-\beta(r_c/r_{1e} - 1)]$. Again, this situation will not arise in the present calculations. Finally, the average shear constant G_e is given by

$$G_e = \frac{2\gamma(\gamma - \beta)}{5\Omega_e}\phi_e . \quad (21)$$

In summary, for a nearest-neighbor fcc EAM model, exponentially decreasing functions have been chosen for the atomistic electron density and the two-body potential, and the energy function of Rose et al. is used. Of the parameters introduced, f_e cancels and r_c plays no significant role in the calculations to be discussed, while the magnitude of β is determined from atomic wavefunction calculations and the resistance to shear of the model gives a relationship involving all three parameters β, γ, and ϕ_e. The cohesive energy, compressibility, and lattice parameter (thus also atomic volume) are given exactly, while the shear anisotropy is fixed at a value of 2.

III. CALCULATIONS

A. Analytic

The energies associated with vacancy formation, divacancy binding, and formation of planar surfaces for fcc metals are dominated by the contributions prior to relaxation. These unrelaxed energies can be calculated analytically with the short-ranged fcc EAM model derived above. Thus the dependence of these energies on the model parameters, to lowest order, can be seen directly.

To create a vacancy, an atom is removed from the interior of the crystal. Twelve two-body bonds are removed, the embedding energy at the equilibrium electron density is removed, and the embedding energy of the 12 neighbors to the vacancy is changed from that at the equilibrium electron density to that at $\frac{11}{12}$ the equilibrium electron density. When the atom is placed on the surface, on average six two-body bonds are formed and the embedding energy at the equilibrium electron density is added. This last energy input seems surprising at first, but the surface is essentially unchanged, so the net effect to the embedding energy is to add one atom to the interior. Detailed counting at the surface yields the same result.

The unrelaxed vacancy-formation energy is therefore given by

$$E_{1v}^{UF} = -12F(\rho_e) + 12F(\tfrac{11}{12}\rho_e) - \Phi_e . \quad (22)$$

Using Eq. (20) to evaluate the embedding terms,

$$F(\rho_e) = -E_c - \Phi_e , \quad (23)$$

$$F(\tfrac{11}{12}\rho_e) = -E_c\left[1 - \frac{\alpha}{\beta}\ln(\tfrac{11}{12}) \right](\tfrac{11}{12})^{\alpha/\beta} - \Phi_e(\tfrac{11}{12})^{\gamma/\beta} ,$$

$$(24)$$

so that the unrelaxed vacancy-formation energy can be written as

$$E_{1v}^{UF} = 12E_c \left[- \left[1 - \frac{\alpha}{\beta}\ln(\tfrac{11}{12}) \right](\tfrac{11}{12})^{\alpha/\beta} \right]$$

$$+ 12\Phi_e(1-(\tfrac{11}{12})^{\gamma/\beta}) - \Phi_e \ . \tag{25}$$

Series expansions can now be made for the various terms in Eq. (25) involving $\tfrac{11}{12}$:

$$\ln(\tfrac{11}{12}) = -(\tfrac{1}{12}) - \tfrac{1}{2}(\tfrac{1}{12})^2 - \tfrac{1}{3}(\tfrac{1}{12})^3 - \cdots \ , \tag{26}$$

$$(\tfrac{11}{12})^{\alpha/\beta} = 1 - \frac{\alpha}{\beta}(\tfrac{1}{12}) + \frac{1}{2!}\frac{\alpha}{\beta}\left[\frac{\alpha}{\beta}-1\right](\tfrac{1}{12})^2$$

$$- \frac{1}{3!}\frac{\alpha}{\beta}\left[\frac{\alpha}{\beta}-1\right]\left[\frac{\alpha}{\beta}-2\right](\tfrac{1}{12})^3 + \cdots \tag{27}$$

with a corresponding equation for $(\tfrac{11}{12})^{\gamma/\beta}$. Assuming α, β, and γ are all of the same magnitude (as they turn out to be on later evaluation), Eq. (25) can be approximated as

$$E_{1v}^{UF} = \tfrac{1}{24}E_c \left[\frac{\alpha}{\beta}\right]^2 \left[1 + \frac{1}{36}\left[3 - 2\frac{\alpha}{\beta}\right]\right]$$

$$+ \Phi_e \left[\frac{\gamma-\beta}{\beta}\right]\left[1 - \frac{1}{24}\frac{\gamma}{\beta} + \frac{1}{864}\frac{\gamma}{\beta}\left[\frac{\gamma}{\beta}-2\right]\right] \ . \tag{28}$$

Finally, using α from Eq. (11) and ϕ_e from Eq. (21),

$$E_{1v}^{UF} = \frac{3}{8}\frac{\Omega_e B_e}{\beta^2}\left\{1 + \frac{1}{12}\left[1 - \frac{2}{\beta}\left[\frac{\Omega_e B_e}{E_c}\right]^{1/2}\right]\right\}$$

$$+ 15\frac{\Omega_e G_e}{\beta\gamma}\left[1 - \frac{1}{24}\frac{\gamma}{\beta} - \frac{1}{864}\frac{\gamma}{\beta}\left[2 - \frac{\gamma}{\beta}\right]\right] \ . \tag{29}$$

Equation (22) can be written as

$$E_{1v}^{UF} = -12E_{12} + 12E_{11} \ , \tag{30}$$

where E_n is defined by

$$E_n = F\left[\frac{n}{12}\rho_e\right] + \frac{n}{12}\Phi_e \ . \tag{31}$$

The details are somewhat more involved, but the unrelaxed divacancy-formation energy in this notation is simply

$$E_{2v}^{UF} = -18E_{12} + 14E_{11} + 4E_{10} \ . \tag{32}$$

Thus the unrelaxed divacancy binding energy is

$$E_{2v}^{UB} = 2E_{1v}^{UF} - E_{2v}^{UF} = -6E_{12} + 10E_{11} - 4E_{10} \ . \tag{33}$$

Making use of the same type of expansions as for the single vacancy, the divacancy binding energy can be converted to an equation which displays the parameter dependence:

$$E_{2v}^{UB} = -\frac{3}{16}\frac{\Omega_e B_e}{\beta^2}\left\{1 + \frac{11}{16}\left[1 - \frac{2}{\beta}\left[\frac{\Omega_e B_e}{E_c}\right]^{1/2}\right]\right\}$$

$$+ \frac{5}{2}\frac{\Omega_e G_e}{\beta\gamma}\left[1 + \frac{1}{8}\frac{\gamma}{\beta} + \frac{11}{864}\frac{\gamma}{\beta}\left[2 - \frac{\gamma}{\beta}\right]\right] \ . \tag{34}$$

The surface energy is determined by dividing the total energy increase in separating bulk material on a crystallographic plane by the total new surface area created. For the three fcc low-index planes, the unrelaxed surface energies are

$$\Gamma_{111}^{U} = \frac{4}{\sqrt{3}a_e^2}(E_9 - E_{12}) \ , \tag{35}$$

$$\Gamma_{100}^{U} = \frac{2}{a_e^2}(E_8 - E_{12}) \ , \tag{36}$$

$$\Gamma_{110}^{U} = \frac{\sqrt{2}}{a_e^2}(E_7 + E_{11} - 2E_{12}) \ . \tag{37}$$

Again expansions are made, and more terms are carried because the convergence of these series is slower than in the vacancy case.

$$\Gamma_{111}^{U} = \frac{4}{\sqrt{3}a_e^2}\left[\frac{9}{32}\frac{\Omega_e B_e}{\beta^2}\left\{1 + \frac{1}{4}\left[1 - \frac{2}{\beta}\left[\frac{\Omega_e B_e}{E_c}\right]^{1/2}\right] + \frac{3}{64}\left[1 - \frac{10}{3\beta}\left[\frac{\Omega_e B_e}{E_c}\right]^{1/2} + \frac{3}{\beta^2}\frac{\Omega_e B_e}{E_c}\right]\right\}\right.$$

$$\left. + \frac{15}{4}\frac{\Omega_e G_e}{\beta\gamma}\left[1 - \frac{1}{8}\frac{\gamma}{\beta} - \frac{1}{96}\frac{\gamma}{\beta}\left[2 - \frac{\gamma}{\beta}\right]\right]\right] \ , \tag{38}$$

$$\Gamma_{100}^{U} = \frac{2}{a_e^2}\left[\frac{1}{2}\frac{\Omega_e B_e}{\beta^2}\left\{1 + \frac{1}{3}\left[1 - \frac{2}{\beta}\left[\frac{\Omega_e B_e}{E_c}\right]^{1/2}\right] + \frac{1}{12}\left[1 - \frac{10}{3\beta}\left[\frac{\Omega_e B_e}{E_c}\right]^{1/2} + \frac{3}{\beta^2}\frac{\Omega_e B_e}{E_c}\right]\right\}\right.$$

$$\left. + 5\frac{\Omega_e G_e}{\beta\gamma}\left[1 - \frac{1}{6}\frac{\gamma}{\beta} - \frac{1}{54}\frac{\gamma}{\beta}\left[2 - \frac{\gamma}{\beta}\right]\right]\right] \ , \tag{39}$$

$$\Gamma_{110}^{U} = \frac{\sqrt{2}}{a_e^2}\left[\frac{13}{16}\frac{\Omega_e B_e}{\beta^2}\left\{1 + \frac{21}{52}\left[1 - \frac{2}{\beta}\left[\frac{\Omega_e B_e}{E_c}\right]^{1/2}\right] + \frac{313}{2496}\left[1 - \frac{10}{3\beta}\left[\frac{\Omega_e B_e}{E_c}\right]^{1/2} + \frac{3}{\beta^2}\frac{\Omega_e B_e}{E_c}\right]\right\}\right.$$

$$\left. + \frac{15}{2}\frac{\Omega_e G_e}{\beta\gamma}\left[1 - \frac{13}{72}\frac{\gamma}{\beta} - \frac{7}{288}\frac{\gamma}{\beta}\left[2 - \frac{\gamma}{\beta}\right]\right]\right] \ . \tag{40}$$

B. Evaluation

For evaluation and interpretation of these equations, copper is chosen as a prototype with the same physical input data as used in earlier EAM calculations:[16] $a_e = 3.615$ Å, $E_c = 3.54$ eV, $B_e = 1.38 \times 10^{12}$ ergs/cm^3, and $G_e = 0.55 \times 10^{12}$ ergs/cm^3. The anisotropy ratio for copper is 3.19, and the slope parameter of the atomic electron density at the nearest-neighbor distance in the crystal, as determined from the Hartree-Fock wave functions,[21] is $\beta = 6.0$ for the $3d^{10}4s^1$ state and $\beta = 6.6$ for the $3d^9 4s^2$ state. Since the $3d^{10}4s^1$ state is expected to dominate, $\beta = 6.0$ is used as a starting value. The shear constant G_e is used as an adjustable parameter instead of ϕ_e, the relationship coming from Eq. (21). Finally, an approximate value of $\gamma = 8.0$ is then required to give the correct magnitude for the single vacancy-formation energy. The embedding function for copper with these parameters is shown as the solid line in Fig. 1. The embedding function is not defined for small electron densities in this model, as mentioned above. For the cutoff distance taken at $r_c = r_{1e} + 3/4(r_{2e} - r_{1e}) = 1.31 r_{1e}$, the embedding function is not defined for $\rho/\rho_e < 0.16$.

With these values, the terms in the expansion for the unrelaxed vacancy-formation energy [Eq. (29)] are

$$E_{1v}^{UF} = 0.106(1 + 0.038) + 1.267(1 - 0.055 - 0.001)$$

$$= 1.306 \text{ eV} . \tag{41}$$

The exact value is 1.305 eV. Convergence is good in both series with the number of terms included and the first term of the second series is clearly dominant in determining the vacancy-formation energy. The bulk modulus and the cohesive energy only affect the first series and thus only play a minor role towards the vacancy-formation energy. Indeed, the cohesive energy enters into the second term in this series, and so its effect is negligible: varying the cohesive energy while holding the other parameters constant does not change the unrelaxed vacancy-formation energy. The second series contributes over 90% of the energy, and scales linearly with the shear modulus or the atomic volume times the shear modulus. The unrelaxed vacancy-formation energy also is approximately inversely proportional to the parameters β and γ.

Many physical parameters, including the bulk modulus, the shear modulus, and the cohesive energy, as well as the vacancy-formation energy, scale roughly with the melting temperature. In one sense, Eq. (29) simply reflects these relationships. However, the significance of this equation is in indicating the dependence of the vacancy-formation energy on these parameters when they do not all scale together. To check if there is any experimental tendency towards the result in the preceding paragraph, the data for six fcc metals tabulated by Foiles et al.[16] was analyzed for the correlation of vacancy-formation energy with various parameters, with goodness of correlation determined by a small value of the ratio of the standard deviation to the average value of the parameter. The sequence from best to worst correlation was ΩC, ΩG, T_m, E_c, C, G, B, $\Omega C'$, C', and ΩB. Thus the atomic volume times the shear modulus does seem to be

of primary importance in determining the vacancy-formation energy, with C more significant than C'.

The results are similar for the other quantities calculated. The corresponding expansion for the unrelaxed divacancy binding energy is

$$E_{2v}^{UB} = -0.053(1 + 0.132) + 0.211(1 + 0.166 + 0.009)$$

$$= 0.184 \text{ eV} , \tag{42}$$

with the exact value being 0.207 eV. While the series convergence is slower here, the shear modulus term is still dominant over the bulk modulus term, although only by a factor of 4. Again, the cohesive energy has little effect on the results, but it is not quite as negligible as in the vacancy-formation case.

The unrelaxed surface energies for the three low-index planes are

$$\Gamma_{111}^U = 225(1 + 0.109 + 0.014) + 896(1 - 0.167 - 0.009)$$

$$= 991 \text{ ergs/cm}^2 , \tag{43}$$

$$\Gamma_{100}^U = 346(1 + 0.145 + 0.025) + 1036(1 - 0.222 - 0.016)$$

$$= 1194 \text{ ergs/cm}^2 , \tag{44}$$

$$\Gamma_{110}^U = 398(1 + 0.176 + 0.037) + 1098(1 - 0.241 - 0.022)$$

$$= 1292 \text{ ergs/cm}^2 . \tag{45}$$

Because of cancellation of positive and negative higher-order terms, these are very close to the exact values of 992, 1195, and 1296 ergs/cm^2, respectively. The sequence from lowest to highest surface energy is $\{111\}$ to $\{100\}$ to $\{110\}$, as expected for the fcc lattice. The pattern is that the lower the surface energy, the better the convergence, and the more the shear modulus term dominates over the bulk modulus term. For the $\{110\}$ surface, almost 40% of the surface energy arises from the bulk modulus term. This is not due to the poorer convergence; including more terms would increase this percentage.

IV. DISCUSSION

The strong dependence of the unrelaxed vacancy-formation energy on the shear modulus occurs because the slope of the embedding function near the equilibrium electron density depends primarily on the slopes of the electron density and the two-body potential near the equilibrium spacing. With Eqs. (30) and (31), the unrelaxed vacancy-formation energy can be approximated by

$$E_{1v}^{UF} = -\Phi_e - \rho_e \frac{dF}{d\rho} \bigg|_e . \tag{46}$$

Furthermore, the equilibrium condition, Eq. (9), can be written as

$$\frac{dF}{d\rho} \bigg|_e = -\frac{d\Phi}{dr_1} \bigg|_e \bigg/ \frac{d\rho}{dr_1} \bigg|_e . \tag{47}$$

Thus the unrelaxed vacancy-formation energy is proportional to Φ_e and, as shown in Eq. (21), Φ_e is proportional to G_e. The slope of the Rose function, Eq. (10), which contains the dependence on the bulk modulus and the

cohesive energy, is zero at equilibrium, and so these parameters do not appear in the equation for the slope of the embedding function with the electron density at equilibrium.

The magnitude of the unrelaxed vacancy-formation energy was used as an input into the model. Based on the dominant first term in the second series, the ratio E_{2v}^{UB}/E_{1v}^{UF} is $\frac{1}{6}$ with this model, the same value as with simple nearest-neighbor bond counting. This ratio decreases to about $\frac{1}{6.3}$ when the exact values are used. Precise experimental data for this ratio are not available, but the present value is realistic.

The surface energies calculated here are smaller than expected. Again, precise experimental values are not available, but, for example. Tyson and Miller report an average surface energy of 1790 ergs/cm^2.[23] An average face should be a mixture of low-energy facets, with the lowest energy {111} predominating, so that the present values are perhaps $\frac{1}{3}$ smaller than the reported value. Furthermore, the calculated value cannot readily be altered by parameter variation while holding the vacancy-formation energy constant. The embedding function is approximately linear near $\rho = \rho_e$. If it were exactly linear, the unrelaxed {111} surface energy would be related to the unrelaxed vacancy formation by

$$\Gamma_{111}^U = \frac{4}{\sqrt{3}a_e^2}\frac{1}{4}E_{1v}^{VF} = 924 \text{ ergs/cm}^2 \ . \tag{48}$$

Again, this is the same relationship as given by simple nearest-neighbor bond counting. The calculated value somewhat greater than this is due to the curvature in the embedding function, but very much greater curvature would be required to attain values comparable to the experimental value. The situation is similar for the other surface energies.

Foiles et al.[16] determined the EAM parameters for six fcc metals using an overdetermined set of experimental data. Since the function given by Rose et al.[20] was used, the atomic volume, cohesive energy, and bulk modulus are fitted exactly. They also used the elastic shears, the vacancy-formation energy, and the heats of solution, where available, for the six metals. In summary, they used 17 parameters and 40 data points in their fitting scheme. Fully relaxed calculations for a variety of defect properties were then carried out with these parameters. A comparison of their results for copper, the present calculations, and experimental results is shown in Table I. The unrelaxed trivacancy and tetravacancy binding energies are also included in this table. As with the divacancy, they are approximately related to the unrelaxed vacancy-formation energy by nearest-neighbor bond counting.

The embedding function for copper used by Foiles et al.[16] is shown as the dashed line in Fig. 1. Also, a square-root dependence, the functional form derived by Finnis and Sinclair,[19] is given as the dotted line. It was pointed out by Daw and Baskes[7] that, for the case in which the embedding function is linear in ρ, the entire scheme is equivalent to using a different pair potential. Indeed, in any model based on Eqs. (1) and (2), i.e., on central two-body forces and a function of a linear superposition of contributions, there is no change whatsoever in the model if terms linear in the superposition variable are added to the embedding functions and corresponding terms are subtracted from the two-body potentials. With a monatomic model, for example, adding $z\rho$ to $F(\rho)$ and subtracting $2zf$ from ϕ does not alter the model. Comparison of the three curves shown in Fig. 1 indicates that, to an excellent approximation, they differ only by a term linear in ρ. Thus the embedding functions in the three models are essentially equivalent. Discussions based on the slope and curvature of the embedding function would therefore seem to be quite general.

Finnis and Sinclair[19] point out that, if the second and higher derivatives of the embedding function are neglect-

TABLE I. Calculated and experimental results. Both sets of calculations use $a_e = 3.615$ Å, $B_e = 1.38 \times 10^{12}$ ergs/cm^3, and $E_c = 3.54$ eV as inputs. The calculations by Foiles et al.[16] are for fully relaxed configurations while the present calculations are for unrelaxed configurations.

	Present	Foiles et al.[a]	Experiment
G_e (10^{12} ergs/cm^3)	0.55[b]	0.54[c]	0.55[d]
$A = C/C'$	2[e]	3.53[c]	3.19[d]
E_{1v}^F (eV)	1.31[b]	1.28[c]	1.3[f]
E_{2v}^B (eV)	0.21	0.27	0.12[g]
E_{3v}^B (eV)	0.62		
E_{4v}^B (eV)	1.27		
Γ_{111} (10^3 ergs/cm^2)	0.99	1.17	
Γ_{100} (10^3 ergs/cm^2)	1.20	1.28	1.79[h]
Γ_{110} (10^3 ergs/cm^2)	1.30	1.40	

[a]Reference 16.
[b]Fitted exactly.
[c]Fitted using an overdetermined set.
[d]Reference 24.
[e]Not adjustable.
[f]Reference 25.
[g]Reference 26.
[h]Reference 23.

ed, the energy changes with their model can be determined solely with an effective pairwise interaction. Foiles[15] has shown more generally that the embedding function can be expanded to yield terms which can be grouped to correspond to one-body, two-body, three-body, etc., factors. The two-body contributions can then be combined with the two-body potential to yield an effective two-body potential. If terms involving second and higher derivatives of the embedding function are neglected, the Finnis-Sinclair result is obtained.

With the present model, if small higher-order terms are dropped, the effective two-body potential is

$$\varphi_{\text{eff}}(r) = \phi_e \left[e^{-\gamma(r/r_{1e}-1)} - \frac{\gamma}{\beta} e^{-\beta(r/r_{1e}-1)} \right] . \quad (49)$$

This is similar to a Morse potential, except that this is one contribution to the energy, whereas the Morse potential is intended to provide the total energy. This effective two-body potential is shown as the solid curve in Fig. 2, together with the corresponding potential from the numerical copper model of Foiles et al.[16] as the dashed curve. The potential from the present model should be forced to zero between first- and second-neighbor distances. These potentials are reminiscent of short-ranged two-body empirical potentials, of which an example for copper[27] is shown as the dotted curve. For metals with small curvature of the embedding function at the equilibrium electron density, these empirical models will closely approximate the embedded-atom method for calculations of energy changes involving small changes in electron density.

V. SUMMARY AND CONCLUSIONS

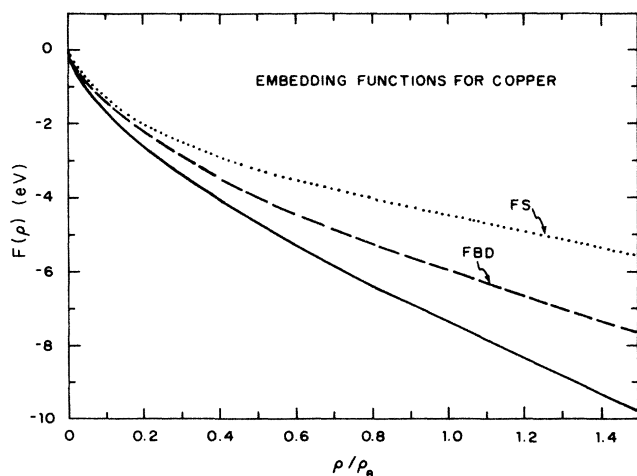A simple nearest-neighbor analytic model for the fcc lattice has been developed which indicates a number of the salient features of the embedded-atom method of computer modeling of metals. The physical inputs into the model are the atomic volume, the cohesive energy, the bulk modulus, the average shear modulus, the vacancy-formation energy, and the slope at the nearest-neighbor distance of the spherically averaged free-atom electron density calculated with Hartree-Fock theory.[21] The model employs an exponential repulsion between nearest neighbors, an exponentially decreasing function for the free-atom electron density, and a universal equation relating the crystal energy and the lattice constant.[20] The anisotropy ratio of the cubic shear moduli is constrained to be 2 with this model.

An analytic function can be obtained for the embedding function, with the slope and curvature at equilibrium electron density given by

$$\left. \frac{dF}{d\rho} \right|_e = - \frac{15\Omega_e G_e}{\beta(\gamma-\beta)\rho_e} , \quad (50)$$

$$\left. \frac{d^2F}{d\rho^2} \right|_e = \frac{9\Omega_e B_e - 15\Omega_e G_e}{\beta^2 \rho_e^2} . \quad (51)$$

The slope of the embedding function at the equilibrium electron density does not depend on B_e or E_c, and the curvature is quite small. The unrelaxed vacancy-formation energy involves changes in energy near equilibrium, and thus is dominated by the slope of the embedding function. This leads to the surprising result that the shear modulus, rather than the bulk modulus or the cohesive energy, is the dominant parameter in determining the vacancy-formation energy. This should hold true for any EAM model based on the energy function given

FIG. 1. Embedding function $F(\rho)$ as a function of the relative electron density ρ/ρ_e. The solid curve is Eq. (20) evaluated for copper, the dashed curve is from a numerical EAM model for copper by Foiles et al. (Ref. 16), and the dotted curve is for $F(\rho)=z\sqrt{\rho}$ as used by Finnis and Sinclair (Ref. 19). Although some variation is found at very low densities, these three curves differ only by a term linear in ρ to an excellent approximation.
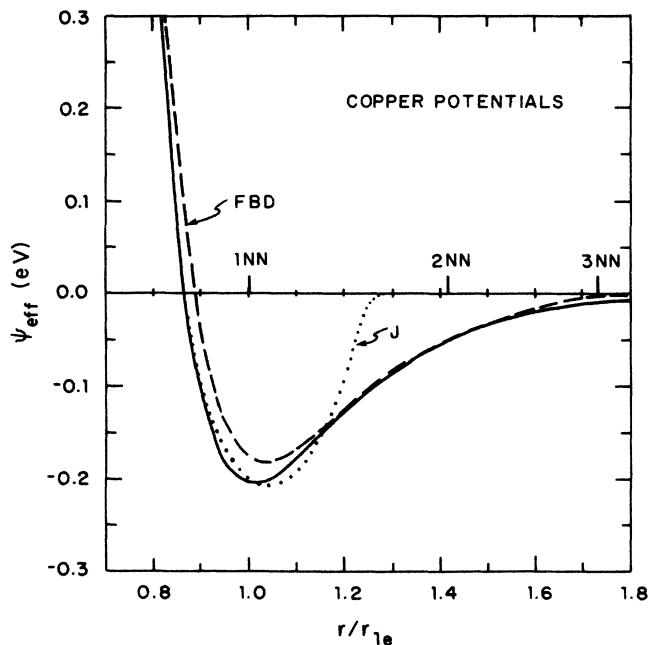

FIG. 2. Effective two-body potentials for copper. The solid curve is Eq. (49) evaluated for copper and is not actually defined past a cutoff range between first- and second-neighbor distances, and the dashed curve is from a numerical EAM model for copper by Foiles et al. (Ref. 16). The dotted curve is a short-ranged empirical two-body potential for copper (Ref. 27).

by Rose et al.[20] and to the extent that this function is an accurate approximation, to any EAM model.

The unrelaxed divacancy binding energy, and the unrelaxed surface energies even more so, contain terms which depend on the embedding function at electron densities significantly smaller than the equilibrium value. Thus the curvature plays a larger role and the shear modulus is not as dominant in these cases.

This may also be seen by expanding the energies for these quantities in rapidly convergent series. The lowest-order terms in these expansions depend only on the slope of the embedding function at the equilibrium electron density, and thus are independent of the bulk modulus and the cohesive energy. In this case, the relations between the various calculated quantities are the same as obtained by simple nearest-neighbor bond counting. For example, the unrelaxed divacancy binding energy is $\frac{1}{6}$ the unrelaxed vacancy-formation energy, and the $\{111\}$ surface energy is $\frac{1}{4}$ the unrelaxed vacancy-formation energy divided by the area per atom on the surface plane. Models based on two-body forces, alone or with volume-dependent energy contributions, will always give bond counting results for unrelaxed configurations.

Daw and Baskes[7] have pointed out that, if the embedding function is completely linear, the contribution from the embedding function can always be converted into a contribution from a two-body potential. Thus it is the curvature of the embedding function which accounts for the "many-body" aspect, or "local volume dependence" of the EAM. This also accounts for the seemingly different character of the embedding function shown in Fig. 1 and Ref. 16 with the earlier reports:[6,7] they differ primarily by a linear term, which can be absorbed into the two-body potential. Furthermore, the embedding functions used by Foiles et al.,[16] the square-root dependence used by Finnis and Sinclair,[19] and the present calculations are shown to differ only by a term linear in the superposition variable, i.e., they are essentially equivalent. The differences in these models occur through the choice of $f(r)$ and $\phi(r)$.

ACKNOWLEDGMENTS

[1]Calculation of the Properties of Vacancies and Interstitials, Natl. Bur. Stand. (U.S). Publ. No. 287 (U.S. GPO, Washington, D.C., 1966).

[2]Interatomic Potentials and Simulation of Lattice Defects, edited by P. Gehlen, J. R. Beeler, Jr., and R. I. Jaffee (Plenum, New York, 1972).

[3]I. M. Torrens, Interatomic Potentials (Academic, New York, 1972).

[4]R. A. Johnson, J. Phys. F 3, 295 (1973).

[5]Interatomic Potentials and Crystalline Defects, edited by J. K. Lee (Metallurgical Society, AIME, Warrendale, Penn., 1981).

[6]M. S. Daw and M. I. Baskes, Phys. Rev. Lett. 50, 1285 (1983).

[7]M. S. Daw and M. I. Baskes, Phys. Rev. B 29, 6443 (1984).

[8]M. J. Stott and E. Zaremba, Phys. Rev. B 22, 1564 (1980).

[9]J. K. Nørskov and N. D. Lang, Phys. Rev. B 21, 2131 (1980).

[10]M. J. Puska, R. M. Nieminen, and M. Manninen, Phys. Rev. B 24, 3037 (1981).

[11]M. I. Baskes, J. Nucl. Mater. 128& 129, 676 (1984).

[12]S. M. Foiles and M. S. Daw, J. Vac. Sci. Technol. A 3, 1565 (1985).

[13]S. M. Foiles, Phys. Rev. B 32, 3409 (1985).

[14]M. S. Daw and R. D. Hatcher, Solid State Commun. 56, 697 (1985).

[15]S. M. Foiles, Phys. Rev. B 32, 7685 (1985).

[16]S. M. Foiles, M. I. Baskes, and M. S. Daw, Phys. Rev. B 33, 7983 (1986).

[17]T. E. Felter, S. M. Foiles, M. S. Daw, and R. H. Stulen, Surf. Sci. 171 L379 (1986).

[18]M. S. Daw, Surf. Sci. 166, L161 (1986).

[19]M. W. Finnis and J. E. Sinclair, Philos. Mag. A 50, 45 (1984).

[20]J. H. Rose, J. R. Smith, F. Guinea, and J. Ferrante, Phys. Rev. B 29, 2963 (1984).

[21]E. Clementi and C. Roetti, At. Data Nucl. Data Tables 14, 177 (1974).

[22]A. D. McLean and R. S. McLean, At. Data Nucl. Data Tables 26, 197 (1981).

[23]W. R. Tyson and W. A. Miller, Surf. Sci. 62, 267 (1977).

[24]G. Simmons and H. Wang, Single Crystal Elastic Constants and Calculated Aggregate Properties: A Handbook (MIT Press, Cambridge, Massachusetts, 1971).

[25]R. W. Balluffi, J. Nucl. Mater. 69& 70, 240 (1978).

[26]A. Seeger and H. Mehrer, in Vacancies and Interstitials in Metals, edited by A. Seeger, D. Schumacher, W. Schilling, and J. Diehl (North-Holland, Amsterdam, 1970), p. 1.

[27]R. A. Johnson, Radiat. Eff. 2, 1 (1969).